

Conformational Analysis: Crystallographic, NMR, and Molecular Mechanics Studies of Flexible Sulfonic Esters

Orde Q. Munro,* Jean M. McKenzie, Sandra D. Strydom, and David Gravestock

School of Chemical and Physical Sciences, University of Natal, Pietermaritzburg,
Private Bag X01, Scottsville 3209, South Africa

munroo@nu.ac.za

Received June 10, 2002

Two novel X-ray structures of the sulfonic ester derivatives 2-(6-iodo-1,3-benzodioxol-5-yl)ethyl 4-nitrobenzenesulfonate, **3**, and 2-(6-iodo-1,3-benzodioxol-5-yl)ethyl 4-methylbenzenesulfonate, **4**, have been obtained in a study aimed at analyzing the structures and conformations of sulfonic ester derivatives that are routinely used in alkaloid syntheses. The crystal structure of **4** is highly unusual, containing four independent molecules that belong to two distinct conformational types: (1) a hairpin conformation (stabilized mainly by intramolecular π -stacking) and (2) a stepped conformation (stabilized mainly by intermolecular π -stacking). Compound **3**, on the other hand, crystallizes exclusively as the hairpin conformer. New MM+ force field parameters for sulfonic esters have been developed using the X-ray data, empirical rules, and DFT calculations to estimate the bond dipole parameters. Grid searches of conformational space for **3** and **4** using MM methods show that there are several gas-phase conformations within 5 kcal/mol of the global minimum and that the lowest energy conformations (by ~ 4.6 kcal/mol) are of the hairpin type. Analysis of the MM conformational energies suggests that the dominant intramolecular interaction stabilizing the hairpin conformations of **3** and **4** is van der Waals attraction. Moreover, the lattice energies for packing the hairpin conformations of **3** and **4** are ~ 4 kcal/mol more favorable than for the stepped conformations. Various intermolecular interactions contribute to the complexity of the observed crystal structures of **3** and **4**, including electrostatic attraction between O and I atoms in neighboring molecules. Langevin dynamics (LD) simulations at several temperatures (6.0 ns, friction coefficient = 2.5 ps^{-1}) indicate that the conformational exchange rates are $\sim 10^{10}$ – 10^{11} s^{-1} over the temperature range 213–400 K, accounting for the temperature-independent ^1H NMR spectra of **3** and **4**.

Introduction

p-Nosylates **1** and their methyl analogues (*p*-tosylates **2**) are well-known sulfonic ester derivatives that have been widely used as coupling reagents in a range of synthetic methodologies due to their inherent lability as leaving groups. The utility of **1** and **2** is exemplified by the many natural product,¹ alkaloid,² and calyx(4)arene³ syntheses that have, as a key step, relied on the use of sulfonic esters.

Despite the important role of sulfonic esters in both synthesis and applied work,⁴ there have been only

limited⁵ conformational studies by NMR spectroscopy of **1** and **2** (with $\text{R}' = \text{sugar}$). This situation is also reflected by the lack of parameters to describe sulfonic esters in established molecular mechanics (MM) force fields such as MM2⁶ and MM3.⁷ The conformational behavior and intra/intermolecular interactions between these ubiquitous groups and other structural components have thus largely been overlooked until now. In this paper, we have attempted to delineate the structures and conformational

(1) (a) Kitaori, K.; Furukawa, Y.; Yoshimoto, H.; Otera, J. *Tetrahedron* **1999**, *55*, 14381–14390. (b) Kitaori, K.; Furukawa, Y.; Yoshimoto, H.; Otera, J. *Tetrahedron Lett.* **1998**, *39*, 3173–3176. (c) Marshall, J. A.; Crute, T. D.; His, J. D. *J. Org. Chem.* **1992**, *57*, 115–123. (d) Sutton, P. W.; Bradley, A.; Farras, J.; Romea, P.; Urpi, F.; Vilarrasa, J. *Tetrahedron* **2000**, *56*, 7947–7958.

(2) (a) Nowak, W.; Gerlach, H. *Liebigs Ann. Chem.* **1993**, 153–159. (b) Pearson, W. H.; Bergmeier, S. C.; Williams, J. P. *J. Org. Chem.* **1992**, *57*, 3977–3987. (c) Denmark, S. E.; Cottell, J. J. *J. Org. Chem.* **2001**, *66*, 4276–4284.

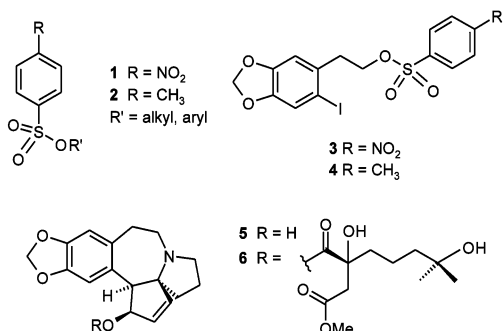
(3) (a) Ferguson, G.; Gallagher, J. F.; Lough, A. J.; Notti, A.; Pappalardo, S.; Parisi, M. F. *J. Org. Chem.* **1999**, *64*, 5876–5885. (b) Arduini, A.; McGregor, W. M.; Pochini, A.; Secchi, A.; Ugozzoli, F.; Ungaro, R. *J. Org. Chem.* **1996**, *61*, 6881–6887. (c) Blanda, M. T.; Farmer, D. B.; Brodbelt, J. S.; Goolsby, B. J. *J. Am. Chem. Soc.* **2000**, *122*, 1486–1491. (d) Burns, D.; Chan, H. K.; Miller, J. D.; Jayne, C. L.; Eichhorn, D. M. *J. Org. Chem.* **2000**, *65*, 5185–5196.

(4) For example: (a) Gabriels, S.; Vanhaver, D.; Vandewalle, M.; Declercq, P.; Viterbo, D. *Eur. J. Org. Chem.* **1999**, 1803, 3–1809. (b) Barilli, P. L.; Catelani, G.; Dandrea, F.; Derensis, F.; Falcini, P. *Carbohydr. Res.* **1997**, *298*, 75–84. (c) Chen, Z.; Fei, S.; Strauss, H. L. *J. Phys. Chem. A* **1997**, *101*, 1640–1645. (d) Kirby, A. J.; Parker, J. K.; Raithby, P. R. *Acta Crystallogr., Sect. C* **1992**, *48*, 832–834. (e) Koch, K. R.; Niven, M. L.; Sacht, C. *J. Coord. Chem.* **1992**, *26*, 161–176. (f) Urata, H.; Miyagoshi, H.; Yumoto, T.; Akagi, M. *J. Chem. Soc., Perkin Trans. 1* **1999**, 1833–1838. (g) Kanagasabapathy, V. M.; Sawyer, J. F.; Tidwell, T. T. *J. Org. Chem.* **1985**, *50*, 503.

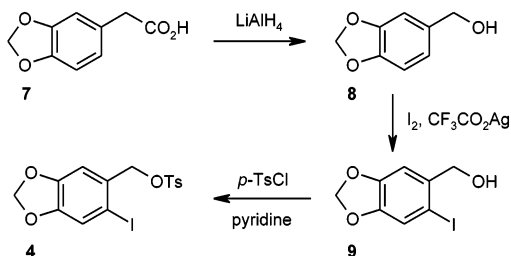
(5) Juaristi, E.; Antunez, S. *Tetrahedron* **1992**, *48*, 5941–5950. (6) (a) Allinger, N. L. *J. Am. Chem. Soc.* **1977**, *99*, 8127–8134. (b) Sprague, J. T.; Tai, J. C.; Yuh, Y.; Allinger, N. L. *J. Comput. Chem.* **1987**, *8*, 581–603. (c) Allinger, N. L.; Kok, R. A.; Imam, M. R. *J. Comput. Chem.* **1988**, *9*, 591–595.

(7) (a) Allinger, N. L.; Yuh, Y. H.; Lii, J.-H. *J. Am. Chem. Soc.* **1989**, *111*, 8551–8566. (b) Lii, J.-H.; Allinger, N. L.; *J. Am. Chem. Soc.* **1989**, *111*, 8566–8575. (c) Lii, J.-H.; Allinger, N. L.; *J. Am. Chem. Soc.* **1989**, *111*, 8576–8582. (d) Allinger, N. L.; Li, F.; Yan, L. *J. Comput. Chem.* **1990**, *11*, 848–867. (e) Allinger, N. L.; Li, F.; Yan, L.; Tai, J. C. *J. Comput. Chem.* **1990**, *11*, 868–895.

SCHEME 1



SCHEME 2



dynamics of the sulfonic ester derivatives **3** and **4**, which are readily available synthons for the 1,3-benzodioxole group found in the skeleton of important alkaloids such as cephalotaxine **5**^{8,9} and its ester derivative homoharringtonine **6** (an anti-cancer drug),¹⁰ primarily to address the paucity of conformational studies of **1** and **2** with synthons that have at least some relevance in the general fields of alkaloid and natural product synthesis (Scheme 1). Since our primary interest is in the structures and conformations of tosylate and nosylate derivatives that contain a 1,3-benzodioxole ring system, a straightforward procedure similar to that reported by Semmelhack^{8a} for the nosylate derivative **3** has been used to synthesize **4** (Scheme 2). Furthermore, the structures of **3** and **4** have been determined from single-crystal X-ray diffraction data for the first time. The crystal structure of **4** is remarkable in that four independent conformations are observed in the asymmetric unit. More importantly, two basic conformational types are evident: (1) a “hairpin” conformation in which the tolyl group lies in van der Waals contact with the 1,3-benzodioxole ring (*intramolecular aromatic stacking*), the sulfonic ester backbone therefore constituting the hairpin chain, and (2) a “stepped” conformer with a more open-chain geometry in which the two terminal ring systems are arranged like a pair of stepping stones (Figure 1).

The complex structure of **4** showing four independent conformations and the distinctly different crystal packing

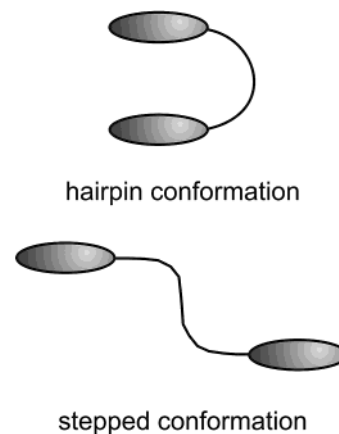


FIGURE 1. Schematic diagram illustrating the basic shapes of the hairpin (π -stacked) and stepped (open-chain) conformations that are accessible to sulfonic esters **3** and **4**.

evident for **3** represent an ideal and intriguing opportunity to develop and check a molecular mechanics force field applicable to these (and related) systems. New force field parameters (MM+) have therefore been developed for sulfonic esters in general and, of specific interest in this work, to study the structures and conformations of **3** and **4** by grid searches of conformational space and Langevin dynamics (LD) techniques. Finally, lattice calculations have been used to elucidate the role played by crystal packing interactions in fine-tuning the solid-state conformations of **3** and **4**.

Results and Discussion

Molecular Structures of 3 and 4. Compounds **3** and **4** crystallize in the triclinic space groups $P\bar{1}$ and $P1$, respectively (Table 1). The unusual asymmetric unit of tosylate **4** comprises four crystallographically unique conformations (**4A–4D**) that belong to the two conformational types illustrated in Figure 1. ORTEP diagrams of one of the stepped and one of the hairpin conformations of **4** are shown in Figure 2 (molecules A and D, respectively). The asymmetric unit of the nosylate derivative **3**, in contrast, comprises a single molecule with a hairpin conformation that is similar in structure to **4D** (Figure 2 and S1). Since **4B** and **4C** are approximate mirror images of **4A** and **4D**, respectively (*vide infra*), their structures are given in the Supporting Information (Figure S2) along with full crystallographic details for the X-ray structures of **3** and **4**. Selected bond distances, bond angles, and torsion angles for **3** and **4** are given in Tables 2–4.

Since an important objective of this work was to develop MM parameters for sulfonic esters in general, we have averaged some of the more relevant chemically unique bond distances, bond angles, and torsion angles for **3** and **4**. Indeed, these data are fundamental to assessing the performance of any computational method for these compounds and, moreover, provide a good estimate of the range of values to be expected since these particular sulfonic esters exhibit multiple conformations. From Table 2, the mean O(sp²)–S(sp³), O(sp³)–S(sp³), C(sp²)–S(sp³), and C(sp²)–I distances measure 1.42(3), 1.57(2), 1.75(2), and 2.09(7) Å, respectively. Similarly, from Table 3 the average I–C(sp²)–C(sp²), C(sp³)–

(8) (a) Semmelhack, M. F.; Chong, B. P.; Jones, L. D. *J. Am. Chem. Soc.* **1972**, *94*, 8629. (b) Semmelhack, M. F.; Stauffer, R. D.; Rogerson, T. D. *Tetrahedron Lett.* **1973**, *45*, 4519. (c) Semmelhack, M. F.; Chong, B. P.; Stauffer, R. D.; Rogerson, T. D.; Chong, A.; Jones, L. D. *J. Am. Chem. Soc.* **1975**, *97*, 2507.

(9) (a) Tietze, L. F.; Schirok, H. *J. Am. Chem. Soc.* **1999**, *121*, 10264–10269. (b) Ikeda, M.; Elbially, S. A. A.; Hirose, K.; Kotake, M.; Sato, T.; Bayomi, S. M. M.; Shehata, I. A.; Abdelal, A. M.; Gad, L. M.; Yakura, T. *Chem. Pharm. Bull.* **1999**, *47*, 983–987. (c) Robin, J. P.; Dhal, R.; Dujardin, G.; Girodier, L.; Mevellec, L.; Poutot, S. *Tetrahedron Lett.* **1999**, *40*, 2931–2934. (d) Tietze, L. F.; Schirok, H. *Angew. Chem., Int. Ed. Engl.* **1997**, *36*, 1124–1125.

(10) Witte, R. S.; Lipsitz, S.; Goodman, T. L.; Asbury, R. F.; Wilding, G.; Strnad, C. M.; Smith, T. J.; Haller, D. G. *Invest. New Drugs* **1999**, *17*, 173–177.

TABLE 1. Crystallographic Data and Structure Refinement Details for **3** and **4**^a

	4	3
empirical formula	C ₁₆ H ₁₅ IO ₅ S	C ₁₅ H ₁₂ INO ₇ S
formula wt	446.24	477.22
<i>T</i> (K)	293(2)	293(2)
wavelength (Å)	0.71073	0.71073
space group	<i>P</i> 1	<i>P</i> 1
<i>a</i> , <i>b</i> , <i>c</i> (Å)	7.816(2), 9.818(2), 23.165(4)	7.363(2), 9.482(2), 13.300(8)
α , β , γ (deg)	82.67(1), 85.47(2), 73.27(2)	76.89(3), 73.99(4), 78.14(2)
<i>V</i> (Å ³)	1686.7(6)	859.2(6)
<i>Z</i>	4	2
<i>D</i> _c (g cm ⁻³)	1.757	1.845
μ_{abs} (mm ⁻¹)	2.044	2.023
unique reflns	6672; <i>R</i> _{int} = 0.0075	3018; <i>R</i> _{int} = 0.0101
data with <i>I</i> > 2 σ (<i>I</i>)	6204	2891
goodness-of-fit on <i>F</i> ²	1.183 ^b	1.117
<i>R</i> indices (<i>I</i> > 2 σ (<i>I</i>))	<i>R</i> ₁ = 0.0394; w <i>R</i> ₂ = 0.1304	<i>R</i> ₁ = 0.0408; w <i>R</i> ₂ = 0.1002
<i>R</i> indices (all data)	<i>R</i> ₁ = 0.0474; w <i>R</i> ₂ = 0.1673	<i>R</i> ₁ = 0.0422; w <i>R</i> ₂ = 0.1010

^a The esd's of the least significant digits are given in parentheses. ^b Absolute structure parameter = 0.26(4).¹¹

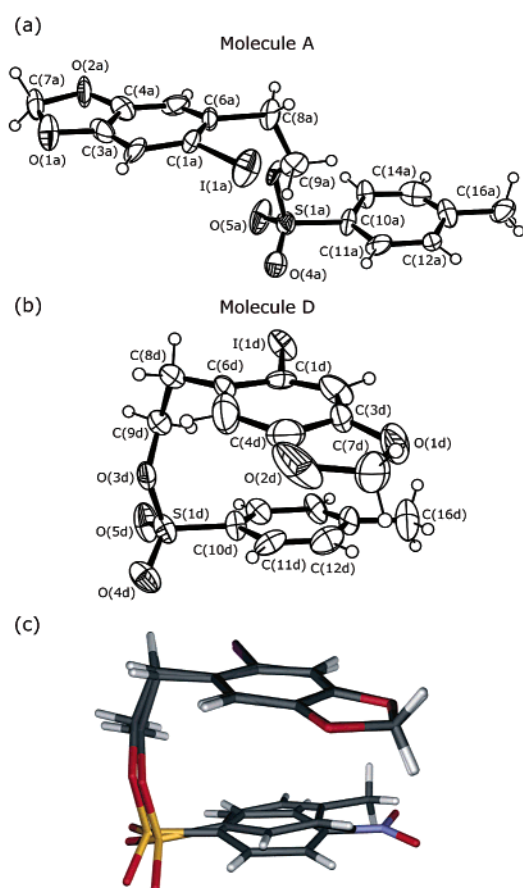


FIGURE 2. Selectively labeled ORTEP diagrams (ellipsoids are drawn at the 30% probability level) of crystallographically unique molecules A (a) and D (b) within the asymmetric unit of **4**. (c) Overlay of the X-ray conformation of **3** and **4D**. The diagram depicts a least-squares fit of the two 1,3-benzodioxole rings (rmsd = 0.083 Å).

O(sp³)–S(sp³), O(sp³)–S(sp³)–O(sp²), O(sp³)–S(sp³)–C(sp²), O(sp²)–S(sp³)–O(sp²), and O(sp²)–S(sp³)–C(sp²) angles measure 119(4), 117(3), 107(3), 104(1), 120(1), and 109(1)°, respectively. These mean bond distances and angles have been used as a starting point in the derivation and optimization of an MM+ parameter set for this class of compounds (vide infra).

TABLE 2. Selected Crystallographic Bond Distances (Å) for Compounds **3** and **4**^a

Tosylate 4			
I(1a)–C(1a)	2.136(17)	S(1a)–O(4a)	1.416(16)
S(1a)–O(5a)	1.467(14)	S(1a)–O(3a)	1.576(11)
S(1a)–C(10a)	1.734(14)	O(3a)–C(9a)	1.41(2)
I(1b)–C(1b)	2.03(2)	S(1b)–O(5b)	1.412(17)
S(1b)–O(4b)	1.358(15)	S(1b)–C(10b)	1.780(16)
S(1b)–O(3b)	1.580(14)	O(3b)–C(9b)	1.55(2)
I(1c)–C(1c)	2.025(19)	S(1c)–O(5c)	1.395(15)
S(1c)–O(4c)	1.419(12)	S(1c)–O(3c)	1.606(13)
S(1c)–C(10c)	1.747(18)	O(3c)–C(9c)	1.42(2)
I(1d)–C(1d)	2.173(15)	O(3d)–C(9d)	1.50(2)
S(1d)–O(4d)	1.418(15)	S(1d)–O(5d)	1.441(15)
S(1d)–O(3d)	1.552(12)	S(1d)–C(10d)	1.722(16)

Nosylate 3 ^b			
I–C(1)	2.108(4)	S–O(5)	1.418(4)
S–O(4)	1.421(4)	S–O(3)	1.558(3)
S–C(10)	1.772(4)	O(3)–C(9)	1.467(6)

^a The esd's of the least significant digits are given in parentheses. The letters a–d designate atoms belonging to molecules A–D, respectively. ^b The atom numbering for compound **3** is equivalent to that for molecule D of **4** for the listed atoms (cf. Figure 2).

The most important torsion angles for the X-ray conformations of **3** and **4** are those involving the flexible sulfonic ester chain that links the 1,3-benzodioxole and benzene ring systems (Table 4). The mean absolute values of the five torsion angles C(10)–S(1)–O(3)–C(9), S(1)–O(3)–C(9)–C(8), C(6)–C(8)–C(9)–O(3), C(1)–C(6)–C(8)–C(9), and O(3)–S(1)–C(10)–C(11) for the two stepped conformations **4A** and **4B** measure 65(3), 171(1), 72(6), 78(5), and 86(14)°, respectively. These same angles average 73(9), 146(2), 66(2), 78(6), and 86(14)°, respectively, for the three hairpin conformers **4C**, **4D**, and **3**. As noted above, **4A** and **4B** are approximate mirror images of one another. This is clearly evident from the reversal in signs of the torsion angles listed in Table 4. The same approximate mirror image relationship exists between **4C** and **4D**.

Conformations **4A** and **4B** have distinct stepped geometries in which the 1,3-benzodioxole ring and tolyl group planes are near parallel and arranged in stepping stone fashion about the sulfonic ester backbone. The dihedral angles between the planes containing the two ring systems measure 6.7° and 10.3° for **4A** and **4B**, respectively. The 1,3-benzodioxole ring is essentially planar in both stepped conformations; the mean absolute

TABLE 3. Selected Crystallographic Bond Angles (deg) for Compounds **3** and **4**^a

Tosylate 4			
O(4a)–S(1a)–O(5a)	121.6(11)	O(4a)–S(1a)–O(3a)	109.1(8)
O(5a)–S(1a)–O(3a)	103.7(8)	O(4a)–S(1a)–C(10a)	107.1(8)
O(5a)–S(1a)–C(10a)	109.0(7)	O(3a)–S(1a)–C(10a)	105.2(7)
C(9a)–O(3a)–S(1a)	119.0(10)	C(6a)–C(1a)–I(1a)	120.6(12)
C(2a)–C(1a)–I(1a)	112.7(13)	C(6b)–C(1b)–I(1b)	121.2(14)
O(4b)–S(1b)–O(5b)	118.3(11)	O(4b)–S(1b)–O(3b)	102.4(8)
O(5b)–S(1b)–O(3b)	109.8(8)	O(4b)–S(1b)–C(10b)	112.7(9)
O(5b)–S(1b)–C(10b)	109.2(9)	O(3b)–S(1b)–C(10b)	103.1(7)
C(9b)–O(3b)–S(1b)	113.5(9)	C(2b)–C(1b)–I(1b)	119.4(13)
O(5c)–S(1c)–O(4c)	121.2(8)	O(5c)–S(1c)–O(3c)	104.1(8)
O(4c)–S(1c)–O(3c)	108.1(7)	O(5c)–S(1c)–C(10c)	109.3(10)
O(4c)–S(1c)–C(10c)	110.1(8)	O(3c)–S(1c)–C(10c)	102.3(7)
C(9c)–O(3c)–S(1c)	121.5(11)	C(6c)–C(1c)–I(1c)	125.2(15)
C(2c)–C(1c)–I(1c)	118.5(12)	C(6d)–C(1d)–I(1d)	117.3(11)
O(4d)–S(1d)–O(5d)	119.7(9)	O(4d)–S(1d)–O(3d)	109.0(9)
O(5d)–S(1d)–O(3d)	103.8(7)	O(4d)–S(1d)–C(10d)	109.1(9)
O(5d)–S(1d)–C(10d)	110.0(9)	O(3d)–S(1d)–C(10d)	104.0(7)
C(9d)–O(3d)–S(1d)	114.2(11)	C(2d)–C(1d)–I(1d)	114.7(13)
Nosylate 3			
O(5)–S–O(4)	120.1(2)	O(5)–S–O(3)	110.9(2)
O(4)–S–O(3)	104.1(2)	O(5)–S–C(10)	108.6(2)
O(4)–S–C(10)	108.6(2)	O(3)–S–C(10)	103.12(18)
C(9)–O(3)–S	118.4(3)	C(6)–C(1)–I	121.4(3)
C(2)–C(1)–I	115.6(3)		

^a The esd's of the least significant digits are given in parentheses. The letters a–d designate atoms belonging to molecules A–D, respectively. ^b The atom numbering for compound **3** is equivalent to that for molecule D of **4** for the listed atoms (cf. Figure 2).

perpendicular deviation of the 9 ring atoms from the mean plane of the fused ring system is 0.04 Å, with O(1a) and C(7b) displaying the largest individual displacements (both 0.09 Å) in molecules A and B, respectively.

As shown in Figure 2, the hairpin conformation of compound **4** differs markedly from the stepped conformation. More specifically, the bridging sulfonic ester chain which links the 1,3-benzodioxole and tolyl rings in **4C** and **4D** adopts a twisted conformation that favors juxtaposition of the two aromatic ring systems and thus leads to individual molecular conformations with well-defined hairpin shapes (Figure 1). The dihedral angle between the planes of the two ring systems in each case measures 14.6° (**4C**) and 15.5° (**4D**). The mean interatomic spacing (shortest contacts) between the atoms of the tolyl ring and those of the 1,3-benzodioxole benzene ring measures 3.6(2) Å for both **4C** and **4D**. This is sufficiently small (and the two ring planes close enough to parallel) to suggest the existence of a stabilizing intramolecular aromatic stacking interaction between the two six-membered rings in each case.^{12,13} We have in fact confirmed this using PM3 calculations (Figure S3), which indicate that a donor–acceptor π – π interaction between the two ring systems is likely (the HOMO resides on the 1,3-benzodioxole ring and the LUMO on the tolyl ring). As noted for **4A** and **4B**, the 1,3-benzodioxole rings of **4C** and **4D** are essentially flat.

Nosylate **3** adopts a hairpin (π -stacked) conformation with a similar geometry to **4D** (Figure 2, Table 4). As

(11) Flack *x*-parameter: (a) Flack, H. D. *Acta Crystallogr., Sect. A* **1983**, *39*, 876–881. (b) Bernardinelli, G.; Flack, H. D. *Acta Crystallogr., Sect. A* **1985**, *41*, 500–511.

(12) (a) Dahl, T. *Acta Chem. Scand. Ser. A* **1975**, *29*, 170. (b) Gavezzotti, A. *Chem. Phys. Lett.* **1989**, *161*, 67. (c) Gavezzotti, A.; Desiraju, G. R. *Acta Crystallogr., Sect. B* **1988**, *44*, 427.

(13) Hunter, C. A.; Lawson, K. R.; Perkins, J.; Urch, C. J. *J. Chem. Soc., Perkin Trans. 2* **2001**, 651–669.

with **4**, the 1,3-benzodioxole ring of **3** is essentially planar (rms deviation = 0.009 Å for all 9 ring atoms) with the largest perpendicular displacement measuring 0.016 Å for C(7). The phenyl group of the nosylate moiety is effectively planar (rms deviation = 0.004 Å). The dihedral angle between the nitro group, which is exactly planar, and the nosylate phenyl group is 2.1°.¹⁴

The dihedral angle between the mean plane of the 1,3-benzodioxole ring and that of the benzene ring measures 6.3°, consistent with a near-parallel arrangement of the ring systems. Interestingly, the two aromatic rings of **3** are aligned closer to parallel than is the case for **4C** and **4D**. The average separation of the phenyl ring atoms from the mean plane of the 1,3-benzodioxole ring is 3.7(1) Å, consistent with a π -stacking interaction between the two groups. The conformation of the sulfonic ester backbone of **3** is similar to that observed for **4D** (Table 4). However, the C(10)–S–O(3)–C(9) dihedral angle for **3** is 14° larger than that for **4D**. This probably reflects differences in the crystal packing of **3** and **4** (vide infra) rather than conformational adjustments to minimize intramolecular steric strain due to the *p*-CH₃ group in **4** since the gas-phase MM-calculated conformations of **3** and **4D** differ negligibly (Figure S4).

Crystal Structures of 3 and 4. Compounds **3** and **4** exhibit significant intermolecular π -stacking interactions in the solid state. As might be expected, the different space groups and asymmetric unit contents for **3** and **4** lead to different types of intermolecular interaction depending on the conformation involved. For concision, and because it straightforwardly illustrates the interesting π – π intermolecular interactions in these systems, Figure 3 shows only the unit cell packing diagram for nosylate **3**. (The crystal packing for tosylate **4** and a discussion of the nonbonded interactions for this compound may be found in the Supporting Information, Figure S5.) Figure 3 depicts a view of the unit cell of **3** approximately parallel to the crystallographic [100] direction. An immediately striking feature of the crystal packing is the arrangement of the molecules into columns of diagonally running hairpin units that are stacked in a back-to-back fashion. There are a number of close nonbonded contacts between the carbon atoms of the ring systems of one hairpin unit and the neighboring units in the columnar stack that are suggestive of intermolecular π – π interactions.^{12,15} For example, contacts less than 3.8 Å occurring between back-to-back 1,3-benzodioxole rings include C(1)⋯C(5)' (3.678(2) Å), C(4)⋯C(6)' (3.647(2) Å), C(4)⋯C(8)' (3.680(2) Å), and C(5)⋯C(6)' (3.633(2) Å). (The atom-numbering scheme for **3** is identical to that for **4D** in Figure 2.) Furthermore, the dihedral angle between the stacked 1,3-benzodioxole rings is exactly zero, consistent with the fact that the crystallographic center of inversion is located between

(14) The out-of-plane tilt of the nitro group is probably an underestimate since the anisotropic temperature factors for the oxygen atoms indicate the possibility of two alternative orientations relative to the plane of the phenyl ring, particularly for O(7), which is the oxygen atom of the nitro group furthest from the reader's view in Figure 2. Use of a disorder model for two alternate C(14)–C(13)–N–O(7) dihedral angles (i.e., O(6) and O(7) positions above and below the plane of the aryl group) slightly lowered (0.02%) the *R* indices, but afforded a poorer description of the geometry of the nitro group. We therefore elected to model the electron density distribution for the nitro group with a single conformation/orientation.

(15) Lokey, R. S.; Iverson, B. L. *Nature* **1995**, *375*, 303.

TABLE 4. Selected Crystallographic Torsion Angles (deg) for Compounds 3 and 4^a

Tosylate 4			
C(10a)–S(1a)–O(3a)–C(9a)	–67(1)	C(10b)–S(1b)–O(3b)–C(9b)	63(1)
S(1a)–O(3a)–C(9a)–C(8a)	–170(1)	S(1b)–O(3b)–C(9b)–C(8b)	172(1)
C(6a)–C(8a)–C(9a)–O(3a)	68(2)	C(6b)–C(8b)–C(9b)–O(3b)	–76(2)
C(1a)–C(6a)–C(8a)–C(9a)	81(2)	C(1b)–C(6b)–C(8b)–C(9b)	–74(2)
O(3a)–S(1a)–C(10a)–C(11a)	96(2)	O(3b)–S(1b)–C(10b)–C(11b)	76(2)
C(10c)–S(1c)–O(3c)–C(9c)	–68(1)	C(10d)–S(1d)–O(3d)–C(9d)	68(1)
S(1c)–O(3c)–C(9c)–C(8c)	147(1)	S(1d)–O(3d)–C(9d)–C(8d)	–148(1)
C(6c)–C(8c)–C(9c)–O(3c)	–63(2)	C(6d)–C(8d)–C(9d)–O(3d)	67(2)
C(1c)–C(6c)–C(8c)–C(9c)	–84(2)	C(1d)–C(6d)–C(8d)–C(9d)	72(2)
O(3c)–S(1c)–C(10c)–C(11c)	102(2)	O(3d)–S(1d)–C(10d)–C(11d)	77(1)
Nosylate 3			
C(10)–S–O(3)–C(9)	82.8(3)	S–O(3)–C(9)–C(8)	–143.9(3)
C(6)–C(8)–C(9)–O(3)	66.9(5)	C(1)–C(6)–C(8)–C(9)	79.4(6)
O(3)–S–C(10)–C(11)	77.8(4)		

^a The esd's of the least significant digits are given in parentheses. The letters a–d designate atoms belonging to molecules A–D, respectively. ^b The atom numbering for compound 3 is equivalent to that for molecule D of 4 for the listed atoms (cf. Figure 2).

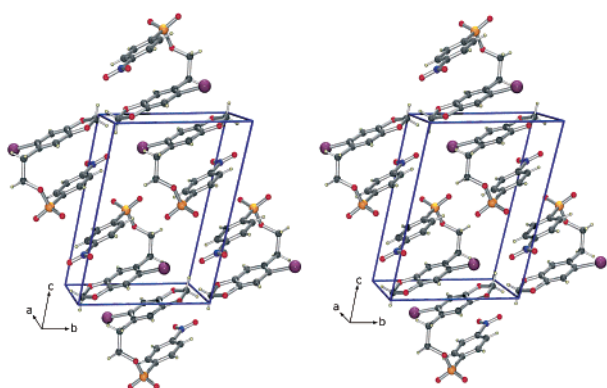


FIGURE 3. Stereoview of the unit cell and closest four neighboring molecules for nosylate 3. The molecules are stacked to form diagonal columns (parallel to the cell diagonal running from [001] to [010]) in which the hairpin conformers are slightly offset from the column center and adopt a zigzag arrangement due to the crystallographically required inversion symmetry.

each pair of rings in the columnar stack. A similar picture prevails for the back-to-back pairs of nitrobenzene rings. Close nonbonded contacts consistent with π – π /aromatic stacking interactions include C(10)···C(11)' (3.783(2) Å), C(10)···C(12)' (3.666(2) Å), C(11)···C(11)' (3.731(2) Å), and C(11)···O(7)' (3.369(1) Å).

The crystal structures of 3 and 4 are the first reported X-ray structures of this class of compounds (sulfonic ester derivatives containing 1,3-benzodioxole and tolyl ring systems). The fact that multiple conformations are observed in the solid state (compound 4) suggests that these molecules are flexible and thus readily adopt a range of conformations at little energy cost. For such a system, the potential energy surface would likely encompass a number of accessible energy minima with relatively low interconnecting barriers. Multiple conformations would presumably also be populated in solution, as is the case for other systems capable of intramolecular aromatic stacking.^{13,16} The intriguing crystal structure of 4 raises several questions. First, how many low-energy conformations are possible and what are the reaction coordinates (conformational pathways) that connect the crystallographically observed structures? Second, what are the energy differences between the hairpin and stepped conformations of 4? Finally, are the energy

barriers between the hairpin and stepped conformations large enough to allow experimental observation of more than one conformation in solution, e.g., by ¹H NMR spectroscopy? The remainder of this paper seeks to answer these questions using a combination of variable-temperature NOE experiments and molecular simulations (MM and LD) to fully elucidate the conformational behavior of this class of sulfonic esters.

Variable-Temperature ¹H NMR Studies. In general, variable-temperature NMR spectroscopy can be used to delineate conformational exchange processes when the barrier between two conformations (the free energy of activation ΔG^\ddagger) is of the order of 5–24 kcal/mol and, perhaps just as importantly, when the conformational isomers are individually distinguishable due to intrinsically different chemical shifts for one or more protons (or other nuclei) in the molecule.^{16b,17,18} We found that the ¹H NMR spectra of 3 and 4 recorded at –60 °C in CDCl₃ or –95 °C in acetone-*d*₆ were equivalent to those recorded at 24 °C (spectra not shown). Moreover, the 1D ROESY spectrum of 4 recorded at –95 °C (irradiation at 5.95 ppm, O–CH₂–O protons) in acetone-*d*₆ showed no NOE enhancements from the tolyl ring protons at 7.29 and 7.71 ppm, consistent with the fact that the hairpin and stepped conformations are still in fast exchange on the NMR time scale even at –95 °C. This suggests that the barriers between the stepped and hairpin conformations of 3 and 4 are <5 kcal/mol in magnitude or that the two conformations are spectroscopically indistinguishable even in the slow exchange limit. The former conclusion is consistent with the detailed conformational energy maps obtained for 3 and 4 by MM and LD methods (vide infra). Moreover, from the number of crystallographically observed conformations of 4 and the fast conformational exchange rate ($k > 10^3$ s^{–1}) implied

(16) For example: (a) Pang, Y.-P.; Miller, J. L.; Kollman, P. A. *J. Am. Chem. Soc.* **1999**, *121*, 1717–1725. (b) Rashkin, M. J.; Waters, M. L. *J. Am. Chem. Soc.* **2002**, *124*, 1860–1861. (c) Martin, C. B.; Mulla, H. R.; Willis, P. G.; Cammers-Goodwin, A. *J. Org. Chem.* **1999**, *64*, 7802–7806. (d) Newcomb, L. F.; Gellman, S. H. *J. Am. Chem. Soc.* **1994**, *116*, 4993–4994. (e) Newcomb, L. F.; Haque, T. S.; Gellman, S. H. *J. Am. Chem. Soc.* **1995**, *117*, 6509–6519. (f) Sindkhedkar, M. D.; Mulla, H. R.; Cammers-Goodwin, A. *J. Am. Chem. Soc.* **2000**, *122*, 9271–9277.

(17) Harris, R. K. *Nuclear Magnetic Resonance Spectroscopy*; Longman Scientific & Technical: Avon, 1986.

(18) Stærk, D.; Norrby, P.-O.; Jaroszewski, J. W. *J. Org. Chem.* **2001**, *66*, 2217–2221.

by the variable temperature NMR studies, **3** and **4** are intrinsically highly flexible compounds.

In Vacuo and Solid-State MM Calculations. The objective of this study was 3-fold: (1) to develop appropriate parameters to calculate the structures of sulfonic esters with the MM+/MM2 force field, (2) to map the full conformational space available to the two esters **3** and **4**, and (3) to use the force field as a basis for an extensive Langevin dynamics study to determine the rates of conformational exchange for these compounds. The lack of parameters for sulfonic esters in the MM+ force field necessitated the development of new bond stretching, angle bending, and torsion angle parameters for this class of compounds from the available crystallographic data. Two types of geometry optimization were performed on the crystallographically observed conformations of **3** and **4** to verify the performance of the augmented MM+ force field: (1) a gas-phase geometry optimization and (2) a separate refinement of each conformation within its lattice environment, i.e., including all neighboring molecule interactions. Selected mean bond lengths, bond angles, and torsion angles for the calculated and observed structures of **4** are compared in Table S7; the level of agreement between the calculated gas phase structural parameters and the X-ray data is good and clearly improves upon inclusion of all neighboring interactions in the solid state (lattice calculation).¹⁹ These results are portrayed graphically in Figure 4, which shows least-squares fits of the MM calculated and crystallographic conformations of **3** and **4**. The average rmsd for the conformations calculated in the gas phase, 0.28(5) Å, is roughly twice as large as that calculated for the conformations within their crystal lattice environment (0.13(3) Å). This suggests that crystal-packing interactions modulate the conformations of **3** and **4** to some extent, as already noted (Figure 3).

The absolute energies of the hairpin and stepped conformations of **3** and **4** are given in Table 5.²⁰ For the tosylate derivative, gas-phase conformations **4A** and **4B** (stepped geometry) are exact mirror images of one another and thus have equivalent strain energies; the same holds true for **4C** and **4D** (hairpin geometry). From Table 5, the hairpin conformation of **4** is more stable than the stepped conformation by 4.29 kcal/mol (gas phase) and 3.7 kcal/mol (solid state). As expected, the solid-state conformations are somewhat more strained than their gas phase counterparts. However, the energy differences amount to <1.2 kcal/mol, consistent with the relatively minor conformational adjustments that are required for optimal packing in the crystal lattice (Figures 3 and 4). The nosylate **3** shows a similar set of energy changes with the hairpin conformation being 4.60 kcal/mol more stable than the stepped conformation in the gas phase. Inspection of the packing energies for the four crystallographically unique conformations of **4** indicates that the two hairpin conformers pack more favorably than the two stepped conformers (by up to ~4.5 kcal/mol). A question

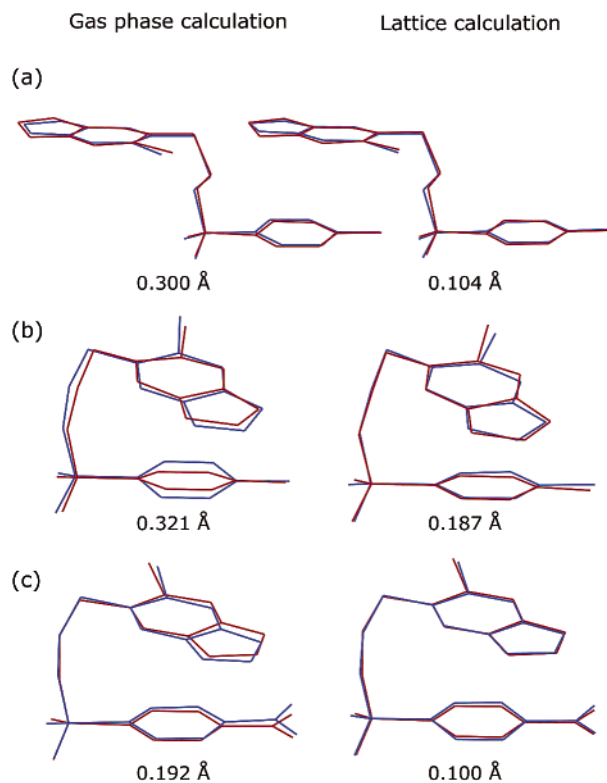


FIGURE 4. Least-squares fits of selected MM calculated (blue) and X-ray (red) conformations of **3** and **4**. Diagrams (a) and (b) are fits for molecules A and D, respectively, of **4**. Diagram (c) shows the fits for the hairpin conformation of **3**. The rmsd values are based on all non-H atoms for both gas phase (left) and crystal lattice geometry optimizations (right).

TABLE 5. Calculated Energies (MM) for Geometry-Optimized Conformations of **3** and **4**^a

conformer	U_T^b (g)	U_T^c (lattice, IA)	packing strain ^d	U_T^e (lattice)	packing energy ^f
4A	5.64	6.17	0.53	-46.64	-52.81
4B	5.64	6.25	0.61	-47.17	-53.42
4C	1.35	2.50	1.15	-53.88	-56.39
4D	1.35	2.51	1.16	-54.69	-57.20
3 hairpin "D" ^g	5.15	6.00	0.85	-51.63	-57.63
3 stepped "A" ^h	9.75				

^a All energies are in kcal/mol. ^b U_T (g) is the total steric energy of the refined gas phase conformation. ^c U_T (lattice, IA) is the single-point energy of the conformation refined in its crystal lattice site after removal of all neighboring molecules. The value of U_T (lattice, IA) is a measure of the *intramolecular* steric energy of a given conformation in the crystal lattice. ^d This term is defined as U_T (lattice, IA) - U_T (g) and gauges the increase in *intramolecular* strain energy associated with packing the conformation in its lattice site. ^e U_T (lattice) is the total steric energy of a given conformer in its crystal lattice site (*intra-* plus *intermolecular* steric energy). ^f The packing energy is defined as U_T (lattice) - U_T (lattice, IA). This term roughly measures the thermodynamic driving force that leads to crystallization of a given conformation. ^g Conformation with a similar geometry to **4D**. ^h Conformation with a similar geometry to **4A**.

that we have yet to unambiguously resolve is why replacement of the *p*-NO₂ group of **3** with a *p*-CH₃ group in **4** leads to a significantly more complicated unit cell comprising an equal ratio of hairpin and stepped conformations. This conformational ratio is unexpected given the higher steric energy of the two stepped conformations of **4** (Table 5) and the conformer distribution observed

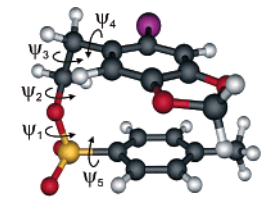
(19) Munro, O. Q.; Madlala, P. S.; Warby, R. A. F.; Seda, T. S.; Hearne, G. *Inorg. Chem.* **1999**, *38*, 4724–4736.

(20) The absolute energies of each conformation are force field dependent. In cases where parameters have been developed to fit experimental heats of formation, the absolute energy of the system may have some physical significance. A more important parameter therefore is the relative energy of two conformations since this suffers less from the choice of parameters used in the force field.

in the LD simulations of this compound (Table 7, *vide infra*). Rather than being purely due to chance, we believe that part of the explanation for the unique solid-state structure of **4** is that the *p*-CH₃ group is involved in (1) fewer and (2) weaker intermolecular interactions than the *p*-NO₂ group of **3**. More specifically, as shown in the packing diagram of Figure 3 (and in somewhat more detail in Figure S6), the *p*-NO₂ group of **3** forms no less than three tight contacts with neighboring atoms in the crystal lattice. Of particular interest are the short, electrostatically favored nitro-O···I' and nitro-N···O' (sulfonic ester) interactions, which measure 3.262 and 3.047 Å, respectively. (The primed atoms are atoms belonging to neighboring molecules in the crystal lattice.) These stabilizing interactions are in fact absent in the tosylate derivative (Figure S7). Their importance as a contributor to the overall lattice energy is apparent if the *p*-NO₂ group of **3** is replaced with a *p*-CH₃ group and the packing energy for the hairpin conformation recalculated. With the present force field, we find that the packing energy for the hairpin conformer of **3** is 0.56 kcal/mol less favorable with the *p*-CH₃ group. Thus, in the case of **4**, which lacks a polar nitro group, cocrystallization of the energetically less favorable stepped conformer may be required to stabilize the lattice *as a whole* by facilitating at least some favorable intermolecular electrostatic interactions. Indeed, inspection of Figure S7 shows that the main electrostatic interaction is between the I atom of **4A** (stepped conformer) and a 1,3-benzodioxole group oxygen atom of **4D** (hairpin geometry) at a distance of 3.332 Å. A similar interaction is observed between molecules **4C** and **4B** (I···O' = 3.447 Å), while the two hairpin conformations **4C** and **4D** behave much like a dimer with I···O' (sulfonic ester) interactions measuring 3.096 and 3.111 Å (Figure S8). The factors governing the exact unit cell contents of **3** and **4** are evidently rather complex and include both the electrostatic interactions discussed above and π - π interactions between the ring systems (*vide supra*). We therefore surmise that there is probably an energy balance between a multitude of intermolecular interactions of varying significance (π -stacking, London forces, dipole-dipole/electrostatic, and van der Waals interactions) and the strain energies of the individual conformers that controls the observed crystal packing in these compounds.

Despite the respectable geometric data obtained with the MM calculations (Figure 4), the question remains as to how accurately the MM+ force field calculates the intermolecular interaction energies in the above systems. Since intermolecular π -stacking interactions are manifest in the crystal structures of **3** and **4**, we chose to test the MM+ force field against the recent high-level *ab initio* calculations on aromatic stacking interactions (benzene···benzene dimer) reported by Tsuzuki et al.²¹ The *in vacuo* MM+ geometry optimized structure of the parallel dimer for benzene (ring systems exactly eclipsed) had a mean plane separation of 3.42 Å and interaction energy of -3.69 kcal/mol. The interaction energy of the benzene dimer with a 3.8-Å mean plane separation was -3.06 kcal/mol. These values compare favorably with the *ab initio* interaction energy (-3.28 kcal/mol) calculated at

TABLE 6. Coordinates and Relative Steric Energies of the Fully Optimized Symmetry Unique Minima ($\Delta U_T \leq 5$ kcal/mol) of **3** and **4**^a



conformer	ψ_1 (deg)	ψ_2 (deg)	ψ_3 (deg)	ψ_4 (deg)	ψ_5 (deg)	ΔU_T (kcal/mol)
4A	295	183	61	86	99	4.29 ^b
4D	77	218	65	85	88	0.00
4E	177	184	58	87	95	3.09 ^b
4F	62	178	179	87	86	3.55 ^b
4G	179	178	181	87	93	3.50 ^b
3A	295	183	61	86	98	4.60 ^c
3D	77	219	66	84	88	0.00
3E	176	185	57	87	95	3.35 ^c
3F	63	178	179	88	86	3.84 ^c
3G	179	178	181	87	91	3.80 ^c

^a The symmetry-related minima B (inverse of A), C (inverse of D), E*, and F* have the coordinates $360 - \psi_n$. ^b Steric energy relative to **4D**. ^c Steric energy relative to **3D**.

the MP2 level of theory at the basis set limit for the parallel stacked benzene dimer with a 3.8-Å ring-ring separation.²¹ The success of the MM calculations in this case may be attributed to the fact that dispersion and nonbonded repulsion, which apparently dominate the π - π interactions in this system (and the aromatic sulfonic esters **3** and **4**), are well accounted for by the Lennard-Jones potential.

Conformational Analysis. To some extent, the data in Table 5 account for the crystallographically observed conformations of **3** and **4**. However, a more complete picture of the conformational space accessible to these systems, particularly the saddle points connecting the energy minima, may be obtained by a combination of dihedral angle (grid) searches of conformational space and MD or LD calculations at several different temperatures. Three of the five sulfonic ester chain torsion angles of compound **4**, ψ_1 - ψ_3 , were selected for conformational analysis, although all five were monitored (Table 6), since they constitute the likely pathway by which the hairpin conformation interconverts to the stepped conformation (and any others not observed in the solid state). Figure 5 shows a plot of the change in steric energy, ΔU_T , as a function of the torsion angles ψ_1 and ψ_3 for compound **4**. Similar conformational energy plots for the torsion angle combinations ψ_2/ψ_3 and ψ_1/ψ_2 of **4** are given in the Supporting Information (Figures S9 and S10, respectively). The coordinates of the lowest energy conformation(s) located from each of these 2D grid searches of conformational space afforded the following average values for the backbone dihedral angles for the symmetry unique *global* minimum energy conformation of **4**: 75, 215, and 60° (ψ_1 , ψ_2 , and ψ_3 , respectively). These dihedral angles are consistent with those of gas-phase structure (b) in Figure 4 (i.e., the hairpin conformation **4D** with ψ_1 , ψ_2 , $\psi_3 = 77, 218, 65^\circ$).

As expected, the conformational energy surface of compound **4** (Figure 5) has a center of inversion at ψ_1 , $\psi_3 = 180, 180^\circ$. Accordingly, there are *five* symmetry

(21) Tsuzuki, S.; Honda, K.; Uchimaru, T.; Mikami, M.; Tanabe, K. *J. Am. Chem. Soc.* **2002**, *124*, 104-112.

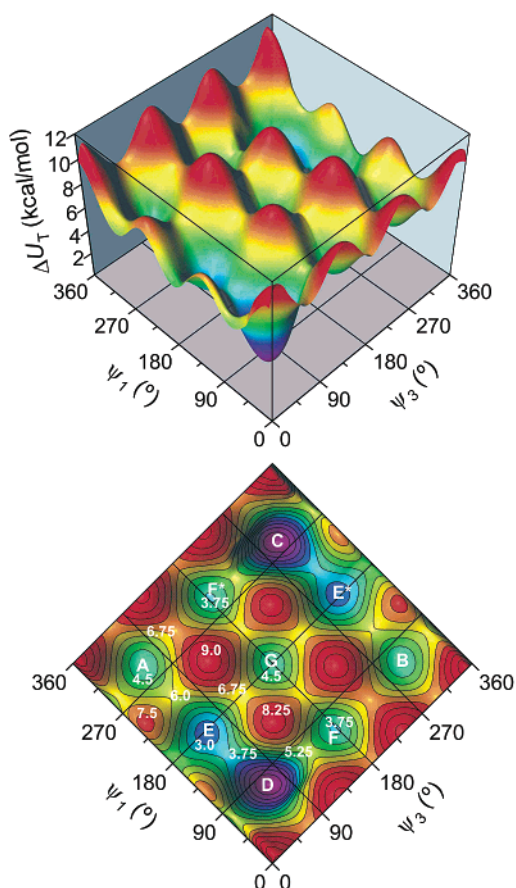


FIGURE 5. Plots of the variation of ΔU_T (kcal/mol) with ψ_1 and ψ_3 for tosylate **4**. The upper plot is a 3D representation of the potential surface; the lower plot is a 2D contour map (contour interval = 0.75 kcal/mol) of the surface with labels for the global and local minimum energy conformations.

unique energy minima on the ψ_1/ψ_3 potential surface (Figure 6). These conformations, marked A–D in Figure 5, are labeled so that they correspond to the X-ray conformations A–D, both in structural type and in designation. Because the surface is centrosymmetric, stepped conformation A ($\Delta U_T = 4.29$ kcal/mol) is mirrored at B and hairpin conformation D ($\Delta U_T = 0$ kcal/mol) is mirrored at C. The local energy minimum E ($\psi_1, \psi_3 = 177, 58^\circ$; $\Delta U_T = 3.09$ kcal/mol) is a stable conformation found along the pathway (reaction coordinate ψ_1) between hairpin conformation D ($\psi_1, \psi_3 = 77, 65^\circ$) and stepped conformation A ($\psi_1, \psi_3 = 295, 61^\circ$).²² As might be anticipated by its coordinates in conformational space relative to A and D, the structure of E is best described as a half-opened hairpin conformation in which the 1,3-benzodioxole ring has swung away from the tolyl ring and is no longer in close van der Waals contact with it. Conformation F ($\psi_1, \psi_3 = 62, 179^\circ$; $\Delta U_T = 3.55$ kcal/mol) lies halfway along the reaction coordinate ψ_3 between hairpin conformation D and the inverted stepped conformation B ($\psi_1, \psi_3 = 65, 299^\circ$). The structure of F is also an opened hairpin conformation. However, the two ring systems are somewhat more splayed than those of E and the relative steric energy of F is correspondingly higher

(22) The symmetry-related counterpart, E*, is equal in energy to conformation E and lies halfway between conformations B and C.

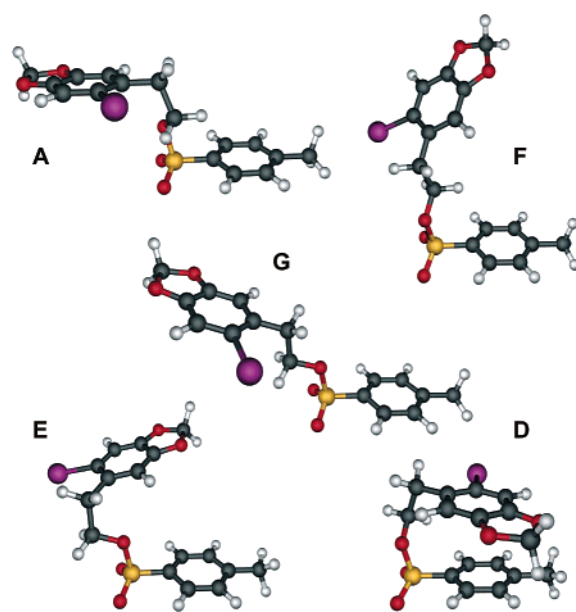


FIGURE 6. Labeled structures of the symmetry unique low energy conformations of **4** taken from the potential energy surface shown in Figure 5.

than that of E. The final low energy structure, conformation G ($\psi_1, \psi_3 = 180, 180^\circ$; $\Delta U_T = 3.50$ kcal/mol), is located at the center of inversion in Figure 5. With both ψ_1 and ψ_3 fully extended, the sulfonic ester chain of conformation G has a staggered, or saw tooth, backbone geometry. Although the 1,3-benzodioxole and tolyl rings are slightly canted relative to one another (16.8°), the structure is clearly a more extended version of stepped conformations A and B. Importantly, Figure 5 confirms that rotations about ψ_1 and ψ_3 are responsible for the crystallographically observed hairpin and stepped conformations of **4** shown in Figures 2 and S2.²³

The ψ_2/ψ_3 and ψ_1/ψ_2 conformational energy surfaces for **4** are given in the Supporting Information (Figures S9 and S10). The global minima from these surfaces are the isoenergetic hairpin conformations C and D, respectively. Moreover, no additional conformations differing from those already located on the ψ_1/ψ_3 surface were found. The dihedral angle coordinates of the symmetry unique minimum energy conformations of **3** and **4** that lie within 5 kcal/mol of the global minimum have been summarized in Table 6. Interestingly, all of the listed minima exhibit ψ_4 and ψ_5 values that fall within 10° of 90° . Indeed, plots of ψ_5 vs ψ_4 as a function of time from the LD trajectories of **4** (vide infra, Figure S11) indicate that ψ_4 and ψ_5 are confined to the values $\pm 90^\circ$ (with a spread of $\pm 30^\circ$ in each case). Table 6 also shows that ψ_2 is limited to a staggered configuration ($180 \pm 40^\circ$) for those conformations that lie within 5 kcal/mol of the global minimum. Stable gauche conformations of ψ_2 are, however, observed with $\psi_2 = 70\text{--}75^\circ$ (Figure S12). There are, in fact, four local minimum gauche ψ_2 conformers

(23) It is important to note that the calculated conformations A and D have isomers B and C which are related through a C_i symmetry element (center of inversion) at $\psi_1, \psi_3 = 180, 180^\circ$. The crystallographically observed isomers of **4** do not display exact inversion symmetry because it is not crystallographically required in the space group P_1 .

that have ψ_4 values of ca. $\pm 90^\circ$ and $\pm 180^\circ$. However, all lie >5 kcal/mol above the global minimum conformation in energy. In the interests of brevity, these have not been tabulated and are not discussed further. Finally, the conformational surfaces for **3** exhibit similar shapes and symmetries to those of **4** (see, for example, Figure S13). However, as shown in Table 6, most of the stable conformations for **3** have relative energies that are ~ 0.3 kcal/mol higher than those of the tosylate derivative. Furthermore, as might be expected, the barriers connecting the energy minima for **3** are ~ 0.3 kcal/mol larger than those of **4**.

Langevin Dynamics Simulations. The conformational energy maps obtained for **3** and **4** indicate (1) that the barriers between the lowest energy structures are of the order of 3–7.5 kcal/mol in the gas phase and (2) that most of the stable minima are within 5 kcal/mol of one another in energy. The system is evidently highly flexible and this raises three interesting questions. First, what are the relative populations of the minima at equilibrium? Second, how large are the rate constants for the associated barrier crossings? Third, at what temperature might conformational interconversions of **3** and **4** be slow enough to allow measurement of the free energy of activation by NMR spectroscopy? These questions may be answered with equilibrium LD simulations because conformational populations are obtained directly from the trajectory and rate constants may be determined from the barrier crossing frequencies at the saddle points of interest for a given temperature.

We originally carried out MD simulations of **3** and **4** at 213, 298, and 328 K using an explicit solvent model (25- \AA^3 solvent box, 113 CHCl_3 molecules) in an attempt to generate MD trajectories that would closely mimic the behavior of these compounds in solution at NMR-accessible temperatures. Contrary to expectation, we found that the lowest energy conformations (C and D) were not the most abundantly populated at 298 and 328 K. Furthermore; only conformations D and E (and not their mirror images C and E*) were significantly populated at 213 K. We suspect that the origin of this physically unrealistic conformational distribution with increasing temperature relates to a problem with the explicit solvent model used, namely that the solute had to be restrained to coordinates within the solvent box to avoid fatal system instabilities that arose when the solute crossed the periodic boundary. (The problem does not arise for small solvent molecules, which correctly cross the periodic boundary with a leaving molecule being instantaneously replaced by its mirror image.) This artificial restraint on the system apparently leads to a sizable damping effect on the conformational exchange process. We therefore chose to use an unrestrained, computationally more efficient nonexplicit solvent model (Langevin method) for all dynamics simulations on compounds **3** and **4** in an effort to delineate the solution-phase dynamic behavior of these compounds.

Figure 7 exemplifies the LD trajectory of **4** at 300 K for the system at equilibrium (115–6015 ps) as a time-graded scatter plot of ψ_1 vs ψ_3 . The conformational distribution is consistent with that expected from the relative energies of the conformations **4A–4F*** mapped in Figure 5 and listed in Table 6. The fractional occupancies of the ψ_1/ψ_3 minima at 300, 350, and 400 K are given

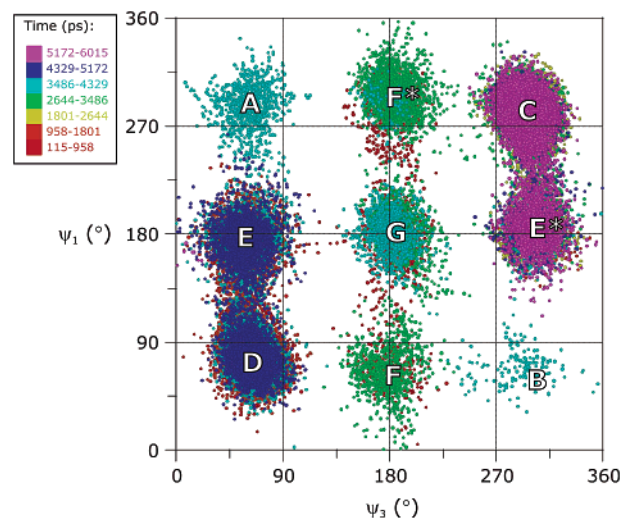


FIGURE 7. Time-graded scatter plot of the conformational distribution of **4** (ψ_1/ψ_3 reaction coordinate) at 300 K. The distribution is from the equilibrated portion of a 6.015 ns Langevin dynamics simulation of **4** (time step = 1.0 fs, friction coefficient = 2.5 ps^{-1} , bath relaxation constant = 0.1 ps, data reduction factor = 1/100).

TABLE 7. Fractional Populations for Conformations of 4 as a Function of Temperature

conformation	300 K	350 K	400 K
4A	0.0131	0.0257	0.00266
4B	0.00243	0.0272	0.0131
4C	0.361	0.207	0.327
4D	0.351	0.359	0.223
4E	0.104	0.0855	0.0819
4F	0.0159	0.0414	0.0364
4G	0.0435	0.134	0.126
4E*	0.0681	0.052	0.131
4F*	0.0407	0.068	0.0590

in Table 7. (The LD trajectory for **4** at 400 K is shown in Figure S14 for comparison.) Notwithstanding some significant population dispersion effects with increasing temperature, particularly between the symmetry-related minima which should have comparable occupancies, we find that the lowest-lying conformations D and C are heavily populated at all temperatures (as expected) with an increasing spread in the values of ψ_1 and ψ_3 clearly evident at higher temperatures. This reflects the greater kinetic energy and thus amplitude of torsional motion within the system at higher temperatures (cf. Figure S14) and, consequently, the higher barrier crossing frequencies for all saddle points on the surface. The minima directly adjacent to D and C (i.e., E and E*) are also well populated (though less so than the global minima due to their somewhat higher relative energies). The time-graded scatter plot of Figure 7 is informative because it shows that the system resides between these two minima for intervals of up to ~ 900 ps. This also explains the population dispersion seen in Table 7—a 6-ns trajectory is probably not quite long enough for a fully symmetric distribution to evolve due to the length of time that the system spends in the lowest energy states.

The conformational exchanges $D \leftrightarrow E$ and $C \leftrightarrow E^*$ exhibit the highest barrier crossing frequencies at all temperatures. To calculate the transition state parameters for at least one main conformational exchange

process in the system, e.g., $D \leftrightarrow E$, we have made use of the fact that the barrier crossing frequency is proportional to the populations of the minima either side of the saddle point. The net number of barrier crossings per unit time can then be weighted according to the relative populations of the minima involved at each temperature. This gave the overall rate constants, k_{overall} , 9.6×10^{10} , 1.5×10^{11} , and $2.6 \times 10^{11} \text{ s}^{-1}$ at 300, 350, and 400 K, respectively (where $k_{\text{overall}} = k_{\text{forward}} + k_{\text{back}}$ and $k_{\text{forward}} = k_{\text{back}}$ at equilibrium). Similar exchange rates have been reported for the trans-gauche isomerization of butane in the liquid phase.²⁴ An Arrhenius plot (Figure S15) of the overall rate constants for the transition $D \leftrightarrow E$ had a slope of $-1183 \pm 143 \text{ K}^{-1}$ and an intercept of 29.3 ± 0.4 ($R = -0.99$). The activation energy for the conformational switch $D \leftrightarrow E$ ($2.3 \pm 0.3 \text{ kcal/mol}$) is roughly 50% of the gas-phase steric energy barrier ($3.75\text{--}4.5 \text{ kcal/mol}$) computed by the dihedral angle driving method for compound **4** in Figure 5. As reported by Kollman's group for a flexible bis(indole) derivative,^{16a} solvation tends to facilitate conformational exchange in such systems by lowering the activation energy barrier through the transfer of kinetic energy to the solute. Extrapolation of the rate constant to $-60 \text{ }^\circ\text{C}$ using the Arrhenius parameters for the system gives a $D \leftrightarrow E$ barrier crossing frequency of $1.9 \times 10^{10} \text{ s}^{-1}$. The rate constant is therefore ~ 6 orders of magnitude faster than can be determined by dynamic ^1H NMR spectroscopy and helps explain the temperature invariant ^1H NMR spectra obtained for **4**, which clearly remains in the fast exchange limit at the temperatures studied.

The remaining conformations A, B, F, F*, and G have temperature-dependent populations that are consistent with their relative energies (Tables 6). The conformational populations obtained from the LD trajectories are useful in a second respect, namely that estimates of the free energy differences between pairs of minima on the potential energy surface are possible. For example, ΔG values for the $E \rightarrow D$ and $E^* \rightarrow C$ transitions at 300 K measure -0.73 and -0.99 kcal/mol , respectively, consistent with the lower steric energies for the two hairpin conformers and thus their significantly higher populations. If we assume that the ΔU_{T} value for this type of conformational transition listed in Table 6 approximates ΔH for the process, i.e., -3.09 kcal/mol , then it is clear that the change in entropy is negative for folding the half-open conformation into the more stable hairpin structure. (Using an average ΔG value of -0.86 kcal/mol for the conformational transition, we calculate that ΔS will be $-7.4 \text{ cal K}^{-1} \text{ mol}^{-1}$ or $-31 \text{ J K}^{-1} \text{ mol}^{-1}$.) Finally, the dynamic behavior of the nosylate **3** is comparable to that of **4** due to the similarity of the potential energy surfaces of these two sulfonic esters.

Conclusions

Two novel X-ray structures of the sulfonic ester derivatives 2-(6-iodo-1,3-benzodioxol-5-yl)ethyl 4-methylbenzenesulfonate, **4**, and the corresponding nosylate 2-(6-iodo-1,3-benzodioxol-5-yl)ethyl 4-nitrobenzenesulfonate, **3**, have been obtained. The tosylate **4** exhibits four

crystallographically independent conformations that fall into two categories, namely, a hairpin conformer in which the two ring systems form a tight intramolecular $\pi\text{--}\pi$ dimer and a stepped (open chain) conformer which shows intermolecular $\pi\text{--}\pi$ interactions with neighboring molecules in the crystal lattice. The nosylate **3**, in contrast, crystallizes in a higher symmetry space group exclusively as the hairpin conformer. A parameter set for use with the MM+ and MM2 force fields has been developed for the first time for sulfonic esters using the X-ray data in conjunction with empirical rules and natural atomic charges to estimate bond dipoles. Molecular mechanics and Langevin dynamics simulations with the modified force field show that there are in fact at least five symmetry-unique conformational types within 5 kcal/mol of the global minimum for both systems but that the hairpin conformers are the most stable by up to $\sim 4.6 \text{ kcal/mol}$ in the gas phase. Overall, **3** and **4** are highly flexible molecules and exhibit conformational exchange rates of the order of 10^{11} s^{-1} —at least 6 orders of magnitude faster than can be measured by dynamic ^1H NMR spectroscopy.

Experimental Section

General Information. Starting materials were obtained from commercial suppliers and were used without further purification, unless otherwise indicated. Radial chromatography was carried out with Merck Silica gel 60 PF₂₅₄. FTIR spectra were recorded at a resolution of 1.0 cm^{-1} as KBr mulls or neat liquids between NaCl plates. ^1H and ^{13}C NMR spectra were recorded on a 500 MHz spectrometer (magnetic field = 11.744 T) using a switchable 5 mm probe. Standard ^1H and ^{13}C pulse sequences were used for 1D and 2D spectra. HRMS data were obtained from the Mass Spectrometry Unit of the Cape Technikon.

2-(1,3-Benzodioxol-5-yl)-1-ethanol, **8**, and 2-(6-iodo-1,3-benzodioxol-5-yl)-1-ethanol, **9**, were synthesized by the standard literature procedure of Semmelhack et al.^{8a} 2-(6-Iodo-1,3-benzodioxol-5-yl)ethyl 4-nitrobenzenesulfonate, **3**, was synthesized from **9** using Tietze's nosylation procedure.²⁵

2-(6-Iodo-1,3-benzodioxol-5-yl)ethyl 4-methylbenzenesulfonate, 4. 2-(6-Iodo-1,3-benzodioxol-5-yl)-1-ethanol **9** (0.512 g, 1.75 mmol) and *p*-toluenesulfonyl chloride (0.50 g, 2.6 mmol) were dissolved separately in a minimal amount of diethyl ether (distilled from sodium benzophenone) and combined. Pyridine (0.5 mL, dried over KOH and distilled) was added to the solution and the mixture left overnight to allow the formation of colorless and yellow crystals. The supernatant liquid was then removed and left to stand allowing more crystals to form. The combined batches of crystals and remaining liquid were partitioned between dichloromethane and water (2:1). The organic layer was separated, washed with ice-cold HCl (5%, 30 mL), dried over MgSO_4 , filtered, and concentrated in vacuo leaving a yellow residue which was purified by radial chromatography (15% ethyl acetate/hexane) giving an oil (0.315 g, 39%). Compound **4** crystallized from the oil on standing. Colorless crystalline product: mp $50\text{--}54 \text{ }^\circ\text{C}$; ν_{max} (KBr)/ cm^{-1} 2900–3000 (CH), 1358 ($\nu_{\text{a}} \text{S(=O)}_2$) and 1176 ($\nu_{\text{s}} \text{S(=O)}_2$), 1248 and 1096 (C–O), 554 (C–I); δ_{H} (500 MHz, CDCl_3) 2.44 (3H, s, Me), 2.98 (2H, t, J 6.9, ArCH_2), 4.16 (2H, t, J 6.9, CH_2OTs), 5.95 (2H, s, OCCH_2O), 6.67 (1H, s, CHCCH_2), 7.13 (1H, s, CHCI), 7.29 (2H, d, J 8.2, CHCMe), 7.71 (2H, d, J 8.2, CHCS); δ_{C} (125 MHz, CDCl_3) 21.61 (Me), 39.81 (ArCH_2), 69.10 (CH_2OTs), 87.78 (CI), 101.67 (OCH_2O), 110.42 (CHCCH_2), 118.64 (CHCI), 127.87 (CHCS), 129.74 (CHCMe), 131.97 (CCH_2), 132.86 (CMe), 144.68 (CS), 147.52 (CCHCCH_2), 148.45 (CCHCI); m/z

(24) (a) Edberg, R.; Evans, D. J.; Morriss, G. P. *J. Chem. Phys.* **1987**, *87*, 5700–5708. (b) Brown, D.; Clarke, J. H. R. *J. Chem. Phys.* **1990**, *92*, 3062–3073.

(25) Tietze, L. F.; Schirok, H.; Wohrmann, M.; Schrader, K. *Eur. J. Org. Chem.* **2000**, 2433–2444.

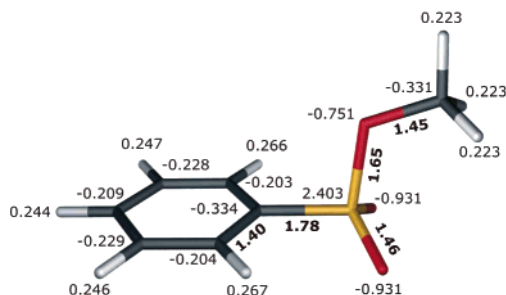


FIGURE 8. Natural atomic charges for methyl benzenesulfonate calculated at the B3LYP/6-31G* level of theory. Bond distances for the unique bonds not involving H atoms are given in boldface type.

(EI) 446 (19, M⁺), 274 (100, M⁺ – HOTs), 261 (29, M⁺ – CH₂OTs) (found M⁺ 455.9682, C₁₆H₁₅O₅SI requires 455.9685).

Crystallography. Single-crystal X-ray data were collected at 295(2) K (Mo K α radiation). The data were reduced with the program XCAD (Oscail V8²⁶) using Lorentz and polarization correction factors. A post-refinement numerical absorption correction (DIFABS²⁷) was applied to the data for **4**. The structures were solved with the direct methods program SHELXS-97.²⁸ The E-maps led to the location of all non-hydrogen atoms; these were refined anisotropically with the program SHELXL-97.²⁸ All hydrogens were included as idealized contributors in the least-squares process with standard SHELXL-97 idealization parameters. The final models were plotted with the program ORTEP.²⁹ Complete crystallographic details, fractional atomic coordinates for all non-hydrogen atoms, anisotropic thermal parameters, fixed hydrogen atom coordinates, bond lengths, bond angles, and dihedral angles for **3** and **4** are available in the Supporting Information. Experimental lattice constants and SHELXL-97 refinement parameters for **3** and **4** are given in Table 1.

DFT Calculations. These were used primarily to obtain estimates of bond dipoles for the new/modified MM+ force field parameter set that we have developed for sulfonic esters. A “parent” derivative, methyl benzenesulfonate (Figure 8), was chosen since it is representative of this class of compounds. Full geometry optimization was effected at the B3LYP³⁰/6-31G* level of theory with the program Titan 1.08³¹ using the following convergence criteria: rms of gradient elements = 3.0×10^{-4} Hartrees/Bohr; rms of nuclear displacement elements = 1.2×10^{-3} Bohr; and energy difference between geometry optimization cycles $< 5.0 \times 10^{-5}$ Hartrees. Accurate partial atomic charges for the sulfonic ester group were obtained via NBO³² analysis of the converged DFT wave function. (The NBO method of partial charge assignment affords basis set independent charge distributions.)

Bond dipoles, μ_D (in debye), were estimated from the natural atomic charge distribution with eq 1

$$\mu_D = \sqrt{\frac{\delta_A}{n} \times \frac{\delta_B}{m}} (1.602 \times 10^{-19}) (d_{AB} \times 10^{-10}) / (3.336 \times 10^{-30}) \quad (1)$$

where δ_A and δ_B are the partial atomic charges on atoms A and B, respectively, n and m are the number of bonds to atoms A and B, respectively, and d_{AB} is the distance between atoms A and B (in Å). The factor 3.336×10^{-30} converts the dipole units from C m to debye. The sign of μ_D is, by definition, positive for the bond A–B when atom B is the negative end of the dipole. Bond dipoles derived with eq 1 are given below as part of the new MM+ force field parameter set for sulfonic esters (vide infra). The natural atomic charges and selected interatomic distances determined at the B3LYP/6-31G* level of theory for methyl benzenesulfonate are given in Figure 8 for completeness. The utility of eq 1 for garnering estimates of bond dipoles for standard S-containing (or indeed any other) functional groups was tested for several simple thioethers, sulfoxides, and sulfones; the values were found to be in agreement with those listed for these functional groups in both the MM2 and MM3 force fields (Supporting Information).

Molecular Mechanics Calculations. HyperChem 6.03³³ (MM+ force field) was used for all calculations. A root-mean-square gradient termination cutoff of 0.01 kcal Å⁻¹ mol⁻¹ was used for geometry optimization with the Polak–Ribiere conjugate gradient algorithm (dielectric constant = 1.5 D). New bond stretching, angle bending, and dihedral angle parameters were developed for the MM+ force field to specifically handle sulfonic esters. Initial estimates of strain free bond lengths, R_0 , and angles, θ_0 , were obtained by averaging the crystallographic values from the conformations of **3** and **4**. Bond stretching force constants, k_s , were derived using Allinger’s method.³⁴ Bond dipoles were estimated using eq 1 (vide supra). Angle bending force constants, k_θ , and torsional parameters, V_n ($n = 1-3$), were estimated from existing MM+ parameters for similar atom sequences. The new parameters were adjusted iteratively until suitable fits of the calculated and observed structures of **3** and **4** were obtained. The final parameter set added to the standard MM+ parameter files was as follows. Bond stretching (bond, k_s /mdyn Å⁻¹, R_0 /Å, μ_D /D): C(sp²)–I, 2.620, 2.090, 1.400; O(sp³)–S(sp³), 4.620, 1.580, –3.073; O(sp²)–S(sp³), 8.412, 1.450, –3.027; and C(sp²)–S(sp³), 3.260, 1.750, –1.563. Angle bending (angle, k_θ /mdyn Å rad⁻², θ_0 /deg): C(sp³)–O(sp³)–S(sp³), 0.770, 110.0; C(sp²)–C(sp²)–S(sp³), 0.550, 121.4; O(sp³)–S(sp³)–C(sp²), 0.700, 103.6; O(sp³)–S(sp³)–O(sp²), 0.560, 106.2; and C(sp²)–S(sp³)–O(sp²), 0.650, 109.6. Torsion angle rotation (dihedral angle, V_1 /kcal mol⁻¹, V_2 /kcal mol⁻¹, V_3 /kcal mol⁻¹): C(sp³)–C(sp³)–O(sp³)–S(sp³), 0.400, 0.520, 0.467; H–C(sp³)–O(sp³)–S(sp³), 0.000, 0.000, 0.530; H–C(sp³)–O(sp³)–S(sp³), 0.000, 0.000, 0.403; C(sp³)–O(sp³)–S(sp³)–O(sp²), 0.000, 0.000, 0.530; C(sp²)–C(sp²)–C(sp²)–S(sp³), –0.270, 9.000, 0.000; C(sp²)–O(sp³)–C(sp³)–O(sp³), 0.000, 5.000, 0.000; C(sp²)–C(sp²)–S(sp³)–O(sp³), 0.000, 0.000, 0.000; C(sp²)–C(sp²)–S(sp³)–O(sp²), 1.243, 1.445, –1.243; and H–C(sp²)–C(sp²)–S(sp³), 0.000, 9.000, 0.000.

Conformational Analysis. Conformational analyses using a standard dihedral angle driving algorithm were carried out by rotating a pair of torsion angles from 0° to 360° in 5° increments with optimization of all remaining internal degrees of freedom at each grid coordinate. Three sulfonic ester chain torsion angles were used to map out the interconversion of the stepped and hairpin conformations of **3** and **4**; ψ_1 , C(sp²)–S(sp³)–O(sp³)–C(sp³); ψ_2 , S(sp³)–O(sp³)–C(sp³)–C(sp³); and ψ_3 , O(sp³)–C(sp³)–C(sp³)–C(sp²). (X-ray structures were used as the starting conformations for these calculations.)

(26) Oscail Version 8: McArdle, P.; Crystallography Center, Chemistry Department, NUI Galway, Ireland. McArdle, P. *J. Appl. Crystallogr.* **1995**, *28*, 65–65.

(27) DIFABS: Walker, N. P.; Stuart, D. *Acta Crystallogr., Sect. A* **1983**, *A39*, 158–166.

(28) SHELXL-97 and SHELXS-97: Sheldrick, G. M. University of Gottingen. (a) Sheldrick, G. M. *Acta Crystallogr., Sect. A* **1990**, *A46*, 467–473. (b) Sheldrick, G. M. *Acta Crystallogr., Sect. D* **1993**, *D49*, 18–23. (c) Sheldrick, G. M.; Schneider, T. R. *Methods Enzymol.* **1997**, *277*, 319–343.

(29) ORTEP3 for Windows: Farrugia, L. J. Department of Chemistry, University of Glasgow, Glasgow G12 8QQ, Scotland, 2001. (a) Farrugia, L. J. *J. Appl. Crystallogr.* **1997**, *30*, 565. (b) ORTEP III: Burnett, M. N.; Johnson, C. K. Oak Ridge National Laboratory report ORNL-6895, 1996.

(30) Becke, A. D. *J. Chem. Phys.* **1993**, *98*, 5648.

(31) (a) Wavefunction, Inc.: 18401 Von Karman Ave., Suite 370, Irvine, CA 92612. (b) Schrödinger, Inc.: 1500 SW First Ave., Suite 1180, Portland, OR 97201.

(32) Weinhold, F. 1999. NBO 4M: Theoretical Chemistry Institute, University of Wisconsin, Madison, WI.

(33) HyperChem 6.03: Hypercube, Inc., 1115 NW 4th St., Gainesville, FL 32601-4256.

(34) Allinger, N. L.; Zhou, X.; Bergsma, J. *THEOCHEM* **1994**, *312*, 69–83.

Langevin Dynamics Calculations. Simulations of the dynamic conformational behavior of **3** and **4** were carried out using a nonexplicit solvent model (Langevin equation) at 300, 350, and 400 K for 6 ns with a 1.0 fs time step at a constant temperature (bath relaxation time = 0.1 ps, friction coefficient = 2.5 ps^{-1}). Each simulation was started at 0 K and then heated to the required temperature over 15 ps in 10 K increments. Selected torsion angles were monitored during each simulation. The trajectories were analyzed with a developmental version of the 32-bit program MDcalc 1.0 that we are currently in the process of writing for population and rate constant analyses of molecular dynamics trajectories.

Acknowledgment. We gratefully acknowledge financial support from the University of Natal (URF) and the National Research Foundation (Pretoria). We would also like to thank Martin C. Watson for his assistance with recording some of our NMR spectra and James Ryan for selecting crystals of **3** and setting up the X-ray data collection for this compound.

Supporting Information Available: ORTEP diagrams of the X-ray structures of each independent molecule of **3** and **4** (Figures S1 and S2, respectively); PM3-calculated frontier

MOs of the hairpin conformer of **4** (Figure S3); root-mean-square fit of the MM-calculated hairpin conformations of **3** and **4** (Figure S4); crystal packing diagram for **4** (Figure S5); crystal packing diagrams highlighting short intermolecular contacts for **3** and **4** (Figures S6–S8); 2D maps of the ψ_2/ψ_3 and ψ_1/ψ_2 conformational energy surfaces of **4** (Figures S9 and S10, respectively); scatter plot of the ψ_5/ψ_4 reaction coordinate from the LD trajectory of **4** at 300 K (Figure S11); minimum energy conformations of the lowest-lying gauche ψ_2 conformers of **4** (Figure S12); plots of the ψ_1/ψ_3 conformational energy surface of **3** (Figure S13); scatter plot of the ψ_1/ψ_3 reaction coordinate from the LD trajectory of **4** at 400 K (Figure S14); Arrhenius plot for the E \leftrightarrow D conformational exchange of **4** (Figure S15); calculations of bond dipole parameters from NBO charge distributions; tables of crystallographic data for compounds **4** (Table S1–S6) and **3** (Table S8–S13); comparisons of MM and X-ray structural data for tosylate **4** (Table S7); complete synthetic details for nosylate **3**; a ZIP file containing PDB files of each energy minimized conformation of **3** and **4**; and a CIF file containing the X-ray structural data for **3** and **4**. This material is available free of charge via the Internet at <http://pubs.acs.org>.

JO0260342